https://doi.org/10.15255/KUI.2021.036
KUI-22/2022
Original scientific paper
Received August 4, 2021
Accepted September 28, 2021

Synthesis and Characterisation of Novel Magnetic Beads as Salicylic Acid Adsorbents from an Aqueous Solution

I. Aroun,[a] *N. Bensacia*,[a,b*] *N. Taoualit*,[b] *L. Djadi*,[b] and *A. Iakhlef*[b]

[a] Laboratoire de Génie Chimique, Université de Blida 1, Bp270 route Soumaa, Blida (9000) Algérie

[b] Laboratoire des applications énergétiques de l'hydrogène, Université de Blida 1, Bp270 route Soumaa, Blida (9000) Algérie

Abstract

The study focuses on the synthesis of two adsorbent forms that were prepared: magnetic nonporous hybrid beads (MNPHB), and magnetic macroporous hybrid beads (MMPHB). The salicylic acid adsorption tests on MNPHB and MMPHB were carried out at a temperature of 25 °C, pH 4, adsorbent mass of 10 mg, and an initial concentration of 10 mg l^{-1}. The adsorption capacity was found to be for MNPHP and MMPHB to 9 mg g^{-1} and 152 mg g^{-1}, respectively. The adsorption kinetic was described by the pseudo-second order model and Freundlich isotherm for the MMPHB beads.

Keywords

Adsorption, salicylic acid, emerging pollutants, urea grafted alginate, cobalt ferrite, magnetic macroporous beads

1 Introduction

Emerging pollutants (EPs) are contaminants that are receiving more and more scientific attention. They may cause fatal effects on humans and aquatic organisms even at very low concentrations.[1] Pharmaceuticals include antibiotics, legal and illicit drugs, *etc*. Nowadays, active pharmaceutical ingredients are bioaccumulating and persistent, which may cause significant consequences for ecosystems.[2] In the pharmaceutical industry, salicylic acid is used as a disinfectant antiseptic agent.[3] In the human body, acetylsalicylic acid is quickly deacetylated forming salicylic acid, which is usually found in surface waters and urban wastewater.[4]

Adsorption is currently one of the most employed separation techniques for industrial water decontamination.[5,6] A wide variety of materials can be used as adsorbents including clays, biopolymers, and other minerals.[7]

Hybrid, "organic-inorganic" biocomposites currently represent a major potential for research work. They are the subject of great benefits, with the properties of inorganic and organic materials at the same time.[8] Spinel ferrite adsorbents are the most suitable option for water decontamination, with high adsorption efficiency and fast kinetics.[9] Encapsulation is an economical and environmentally friendly process for immobilizing a material within a hydrogel matrix, thus retaining their adsorption properties, and facilitating their separation process from aqueous solutions.[10]

The most popular anionic polysaccharide used for beads preparation is alginate. It is constituted of (1-4)-linked β-D-mannuronate (M) and α-L-guluronate (G) residues. The grafting of urea on alginate structure leads to the creation of new reactive groups that will bring additional reactivity or selectivity: these new reactive groups may increase sorption capacity of the biopolymer.[11] The main objective of the present work was the synthesis of novel magnetic hybrid beads, prepared with urea grafted alginate and cobalt ferrite in order to remove salicylic acid from contaminated water. Two adsorbent forms were prepared: magnetic nonporous hybrid beads and magnetic macroporous hybrid beads. The creation of porosity on the magnetic hybrid beads is a critical factor that influences sorption properties.[11]

2 Experimental

2.1 Materials

Ferrous chloride tetrahydrate ($FeCl_2 \cdot 4\ H_2O$, (97 %, Riedel-de Haën), and cobalt chloride ($CoCl_2 \cdot 6\ H_2O$, Biochem) were used for the synthesis of cobalt ferrite ($CoFe_2O_4$). Sodium alginate ($C_6H_7NaO_6$, Panreac AppliChem), urea (NH_2CONH_2, 99.0–100.5 %, Panreac AppliChem), calcium chloride ($CaCl_2$, ≥ 99 %, Biochem), calcium carbonate ($CaCO_3$, Merck, ≥ 99 %), and hydrochloric acid (HCl, 36.5 %, Merck) were employed in the preparation of beads. Salicylic acid ($C_7H_6O_3$, Sigma-Aldrich) was also used. The protocol according to *Dehghani et al*.[12] was used to prepare cobalt ferrite.

2.3 Preparation of alginate and urea grafted alginate beads

Alginate beads were synthesised according to the following protocol.[13] Alginate solution of 3.4 % w/v was prepared. A two-step technique was used to prepare grafted alginate beads. Firstly, an amount of 3.000 g of sodium alginate was dissolved in 84 ml of distilled water in the presence of 1.116 g of urea. The mixture was heated at 50 °C for 3 h under reflux. Following the same technique, the chemical-

* Corresponding author: Nabila Bensacia, PhD
Email: bensacianabila@yahoo.fr

ly grafted alginate solution was dropped into the ionotropic gelation solution $CaCl_2$ (0.2 M).

2.4 Preparation of MNPHB prepared with urea grafted alginate and $CoFe_2O_4$

The ionic gelation method was employed to prepare nonporous hybrid beads according to *Zhao et al*.[10] A mixture of urea grafted alginate (1 % w/w) and $CoFe_2O_4$ (1 % w/w) was injected drop-by-drop through a tiny nozzle into 0.3 l of $CaCl_2$ (0.2 M) solution. The ionotropic gelation process was maintained overnight under moderate agitation before being washed multiple times with distilled water. Urea grafted alginate/$CoFe_2O_4$ nonporous hybrid beads were dried in an oven at 40 °C.

2.5 Preparation of MMPHB with urea grafted alginate and $CoFe_2O_4$

A homogeneous solution was prepared with a mixture of urea grafted alginate (1 % w/w), $CoFe_2O_4$ (1 % w/w), and $CaCO_3$ (1 % w/w).[14,15] It was then injected drop-by-drop through a tiny nozzle into 0.3 l of $CaCl_2$ solution (0.2 M). The $CaCO_3$ was removed from the beads by immersing them in a hydrochloric acid solution (0.5 M) bath for 40 min. After that, the beads were washed multiple times using distilled water and dried in an oven at 40 °C.

2.6 Characterisation of the prepared materials

The samples were characterised using Fourier Transform Infrared Spectroscopy (FTIR) by FTIR-8900 instrument (Shimadzu). The crystalline structure of the prepared beads was analysed by Rigaku SmartLab high-resolution X-ray diffractometer (XRD). The pH_{pzc} (point of zero charge) of the two adsorbents was determined by potentiometric dosage.[16] Size, morphology, and porosity of the beads were determined by Scanning Electron Microscopy (SEM) associated with Energy Dispersive X-ray microanalysis EDX (Quanta 650, Bruker).

2.7 Adsorption studies

Salicylic acid adsorption on the hybrid beads was carried out in a thermostated cell. To 10 ml of salicylic acid aqueous solution (10 mg l^{-1}), an amount of 10 mg of adsorbent was added. The pH was adjusted to the targeted value using HCl (0.1 M) and NaOH (0.1 M). The effects of pH (2 to 14), adsorbate initial concentration (10 to 100 mg l^{-1}), and mass of adsorbent (10 to 120 mg) on the adsorption behaviour were studied. The residual concentration of adsorbate was determined after magnetic filtration and analysed on ultraviolet/visible spectrophotometer UV-1800 (Shimadzu) at λ_{max} = 296 nm. The adsorption kinetics were studied by measuring the change of concentration of salicylic acid with time. The adsorption capacity, Q_e (mg g^{-1}), was calculated using the Eq. (1):

$$Q_e = \frac{c_0 - c_e}{W} \cdot V \tag{1}$$

where c_0 and c_e are the initial and equilibrium concentrations of salicylic acid (mg l^{-1}), respectively, V is the volume of the solution (l), and W is the weight of the adsorbent (g).

2.7.1 Adsorption kinetics

The salicylic acid adsorption kinetics data were analysed by testing pseudo-first order and pseudo-second order kinetic models with ORIGIN 2018. The pseudo-first order model can be expressed by Eq. (2):

$$\ln(q_e - q_t) = \ln(q_e) - K_1 t \tag{2}$$

where q_e is amount of salicylic acid adsorbed at equilibrium state (mg g^{-1}), q_t is amount salicylic acid adsorbed at time t (mg g^{-1}), and K_1 is rate constant (min^{-1}) of pseudo-first order. The pseudo-second order model can be expressed by Eq. (3).

$$\frac{t}{q_t} = \frac{1}{K_2 q_e^2} + \frac{1}{q_e} t \tag{3}$$

One again, q_e is amount of salicylic acid adsorbed at equilibrium state (mg g^{-1}) and q_t the amount of salicylic acid adsorbed at time t (mg g^{-1}). K_2 rate constant (g mg^{-1} min^{-1}) of pseudo-second order. The parameters of pseudo-first and pseudo-second order kinetics are shown in Table 1.

2.7.2 Adsorption isotherms

The adsorption isotherm experiments were accomplished by shaking 10 ml of salicylic acid solutions of different concentrations (10–100 mg l^{-1}) with 10 mg of adsorbent for 1 h, at pH 4 and 25 °C. The adsorption isotherm shows how the adsorbed molecules are distributed between the liquid and solid phases at equilibrium. The isotherms of Freundlich and Langmuir were studied to describe the salicylic acid adsorption.

2.7.2.1 Freundlich model

Freundlich isotherm is commonly used to describe the adsorption processes for the heterogeneous surface.[17] It was applied to represent the multi-layer adsorption.[18] The nonlinear and linear forms of the Freundlich model are provided by the Eqs. (4) and (5).

$$q_e = K_f c_e^{\frac{1}{n}} \tag{4}$$

$$\log q_e = \log K_f + \frac{1}{2} \log c_e \tag{5}$$

The amount of salicylic acid adsorbed per gram of the adsorbent at equilibrium state is marked as q_e (mg g^{-1}), c_e is the equilibrium concentration of adsorbate (mg l^{-1}), K_f is Freundlich isotherm constant (mg g^{-1}) that approximately indicates adsorption capacity, and n is adsorption intensity which is a function of the adsorption strength.[16]

2.7.2.2 Langmuir model

This model describes the formation of a monolayer adsorbate on the external surface of the adsorbent; no further adsorption subsequently occurs.[19] It is valid for monolayer adsorption onto a surface containing a finite number of identical sites. Langmuir model is represented by Eq. (6):

$$q_e = \frac{q_{max} K_L c_e}{1 + K_L c_e} \quad (6)$$

where c_e represents the adsorbate equilibrium concentration (mg l^{-1}), q_e is the amount of the salicylic acid adsorbed *per* gram of the adsorbent at equilibrium state (mg g^{-1}), q_{max} is maximum monolayer coverage capacity (mg g^{-1}), and K_L is Langmuir isotherm constant (l mg^{-1}).

2.7.3 Error analysis

Error analysis offers a rigorous tool for computing adsorption parameters *via* isotherm models. Several functions are used for this purpose. The sum of squares of the errors, SSE (Eq. (7)), was used in this study.[20]

$$SSE = \sum (q_{calc} - q_{exp})^2 \quad (7)$$

Calculated and experimentally determined values are marked with indices calc and exp, respectively.

3 Results and discussion

Several tests were carried out in order to highlight the magnetic properties of the prepared beads. The test showed that our adsorbents were attracted to the magnet, which confirmed the magnetic properties.

3.1 Adsorbent characterisation

3.1.1 Fourier Transform Infrared Spectroscopy

Fig. 1 shows the FTIR spectra of sodium alginate, and urea grafted alginate beads. The grafting of urea in the structure of alginate was confirmed by the appearance of the two strong peaks at 3739.72 cm^{-1} and 3556.49 cm^{-1}; assigned to two N−H stretching vibrations, which replace the broad

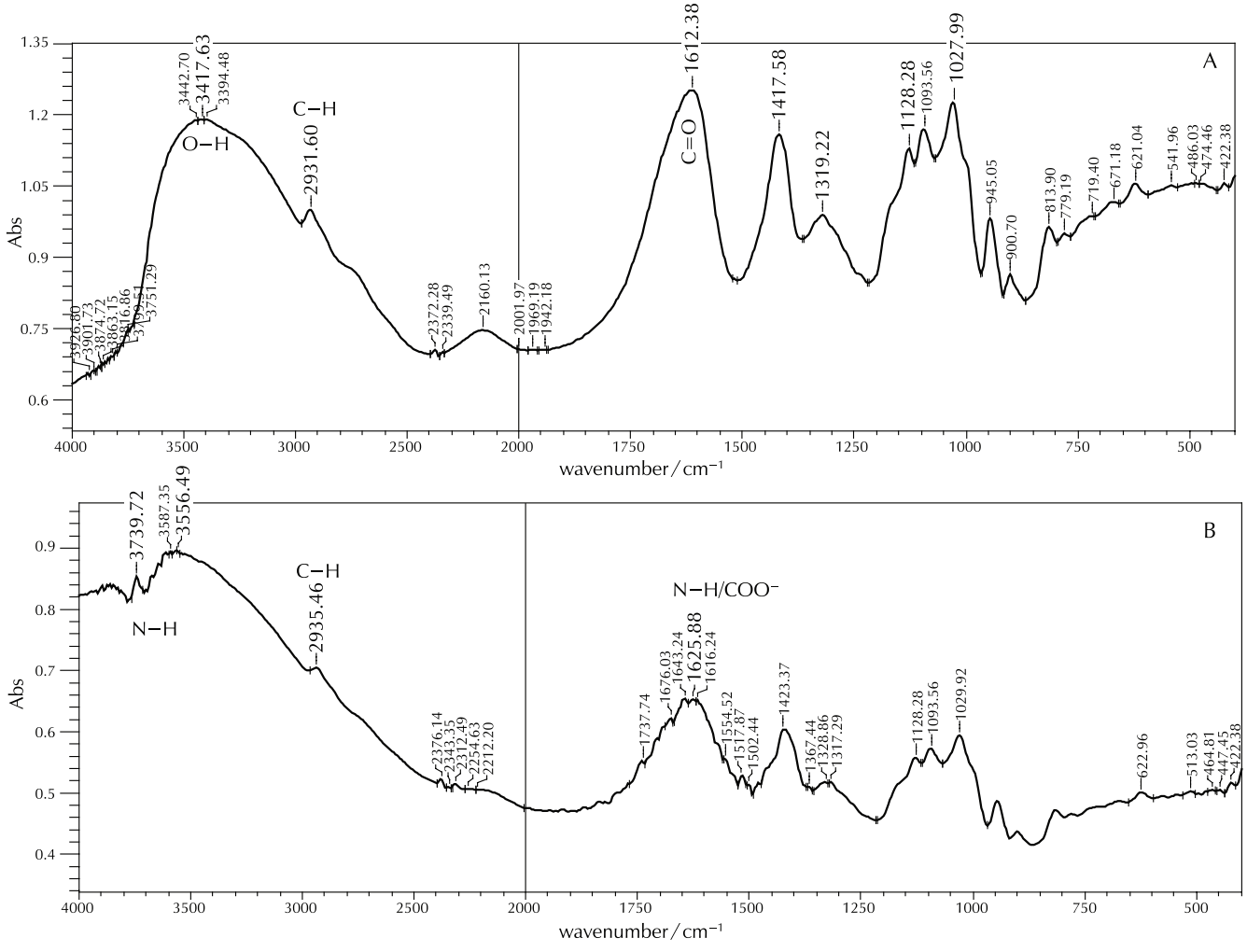

Fig. 1 – FTIR spectra of sodium alginate beads without urea (A) and with urea (B)

band at 3417.63 cm^{-1} associated to O−H stretching vibrations of alginate. On the sodium alginate beads spectrum without urea (A), the peak that was attributed to the vibration of C−H was obvious at 2931.60 cm^{-1}, the wavenumbers located at 1612.38 cm^{-1}, 1417.58 cm^{-1}, 1319.22 cm^{-1}, 1128.26 cm^{-1}, and 1027.99 cm^{-1}, corresponded respectively to asymmetric C=O carboxylic groups: combination of O−C−O symmetrical elongation vibrations, and C−OH deformation vibrations: characteristic band of the deformation vibrations of the C−C−H and O−C−H bonds: characteristic band of vibrations of elongation of C−O groups: characteristic band of vibrations of elongations of C−O and C−C bonds. The peaks situated at 945.05 cm^{-1} and 813.90 cm^{-1} are typical vibrations of uronic acids.[21]

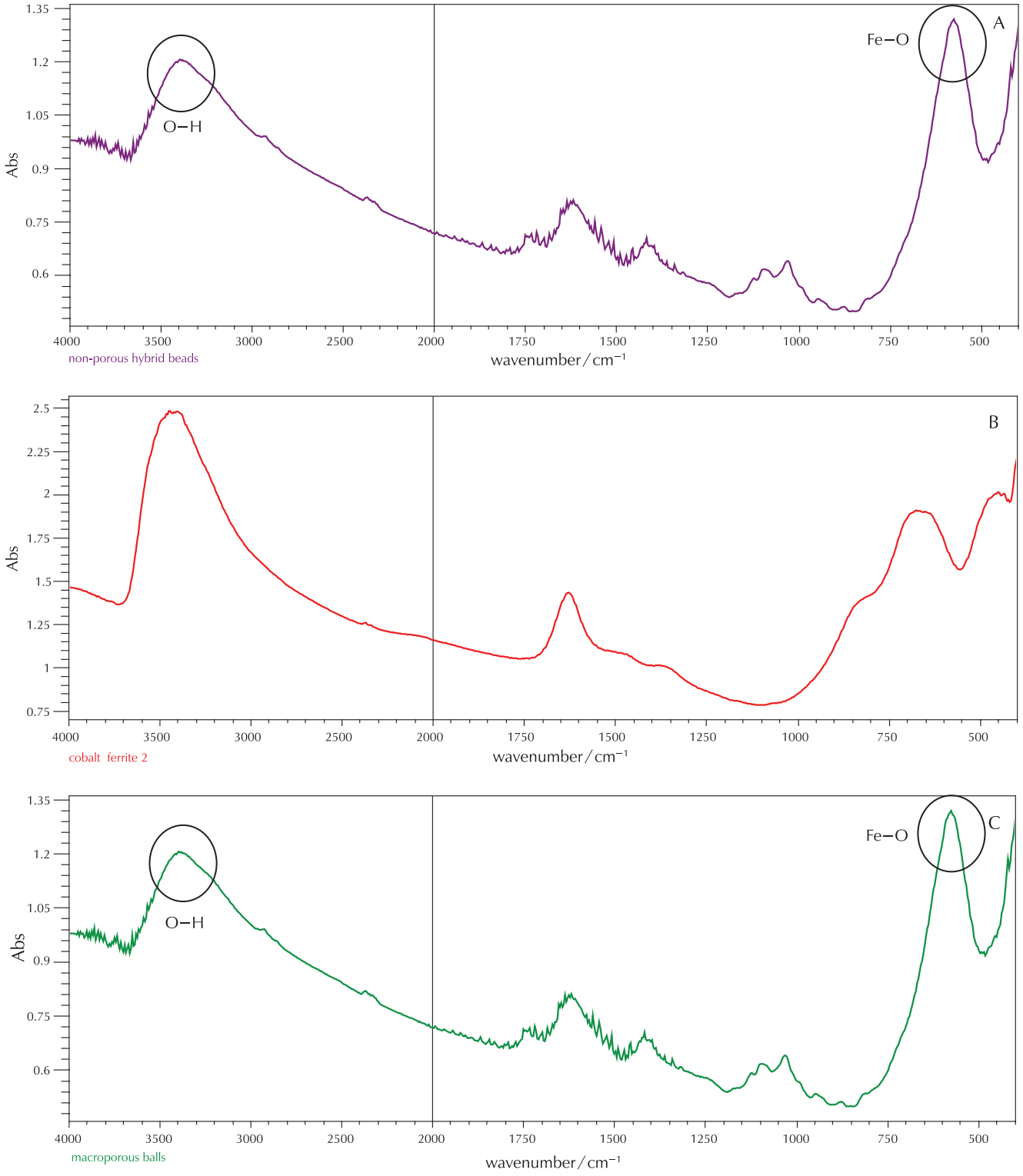

Fig. 2 – FTIR spectra of: A) MNPHB, B) $CoFe_2O_4$, and C) MMPHB

On the urea grafted alginate spectrum (B), the peak located at 1625.88 cm^{-1} was assigned to carboxylate band N−H/COO^-. The wavenumbers located at 1423.37 cm^{-1} and 1128.2 cm^{-1} respectively corresponded to: C−O of alginate with the contribution of C−N stretching and deformation vibrations of primary amine groups. The peak recorded at 1029.92 cm^{-1} indicated the combination of several bands associated to: C−N and C−O stretching vibrations and C−O−C (pyranose unit).[22]

Fig. 2 shows the FTIR spectra of MNPHB, $CoFe_2O_4$, and MMPHB. On the cobalt ferrite spectrum, peaks at 3440.77 cm^{-1} and 1629.74 cm^{-1} were attributed to the stretching modes and bending vibration of the absorbed or free water.[12] Both MNPHB and MMPHB FTIR spectra presented peaks at 574.75 cm^{-1} and 418.52 cm^{-1} assigned to the tetrahedral and octahedral Fe−O bonds, respectively. These results are consistent with the work of *Aroun et al*.[5]

3.1.2 X-ray diffraction

In order to determine crystal phase of the magnetic biocomposites, the dried and crushed samples were analysed using XRD in the region of 2θ between 8 and 80°. The XRD patterns of sodium alginate, nonporous (alginate/$CoFe_2O_4$), macroporous (alginate/$CoFe_2O_4$), and MMPHB (urea grafted alginate/$CoFe_2O_4$) beads are shown in Fig. 3. Alginate beads presented two typical crystalline diffraction peaks at 13.50° and 22.60°.[17] From the XRD patterns, it can be noted that all the magnetic hybrid beads showed different characteristic peaks assigned for $CoFe_2O_4$ located at 2θ (16.97°, 26.68°, 30.00°, 31.91°, 35.24°, 42.90°, 53.38°, and 56.83°).[23]

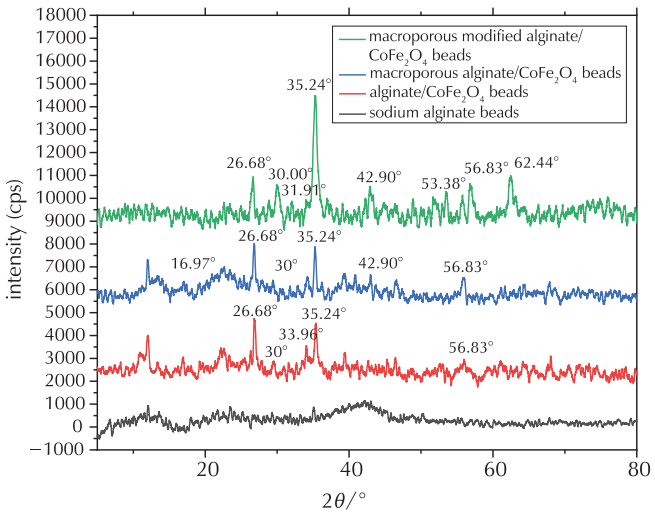

Fig. 3 – XRD pattern of sodium alginate, alginate/$CoFe_2O_4$, macroporous alginate/$CoFe_2O_4$, and MMPHB beads

3.1.3 Determination of the point of zero charge

The point of zero charge pH_{pzc} is the parameter corresponding to the pH for which the adsorbent surface has a zero charge. This method is based on the plot of $Q_S = f(pH)$ (Fig. 4), and the intersection point between the curve and the x-axis ($Q_S = 0$) was determined by Origin. The isoelectric point was determined at $pH_{pzc} = 7.02$ for MNPHB and at $pH_{pzc} = 8.5$ for MMPHB. The surface is positively charged when the pH value is below pH_{pzc} and negatively charged when it is above of pH_{pzc}.[16]

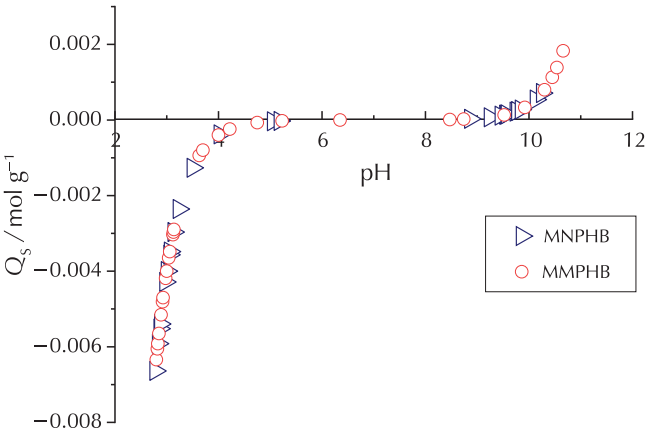

Fig. 4 – Potentiometric titration curve of MNPHB and MMPHB

3.1.4 Scanning Electron Microscopy

The magnetic macroporous MMPHB beads were analysed by SEM. The porous structure is shown in Fig. 5. The prepared beads with approximately 1.854–2.501 mm diameter featured many heterogeneous macropores with medium diameters ranging from 90.52 µm to 132.6 µm. These macropores were created because of $CaCO_3$ dissolution in the acidic mixture (HCl) used for beads preparation with CO_2 gas generation. This subsequently generated the formation of bubbles inside the beads during gelation with calcium ions of $CaCl_2$ solution, then produced macroporous beads.[23]

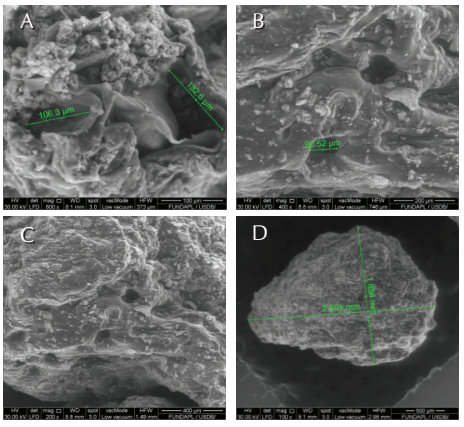

Fig. 5 – SEM images of MMPHB (urea grafted alginate/$CoFe_2O_4$) magnified 800× (A), 400× (B), 200× (C), and 100× (D)

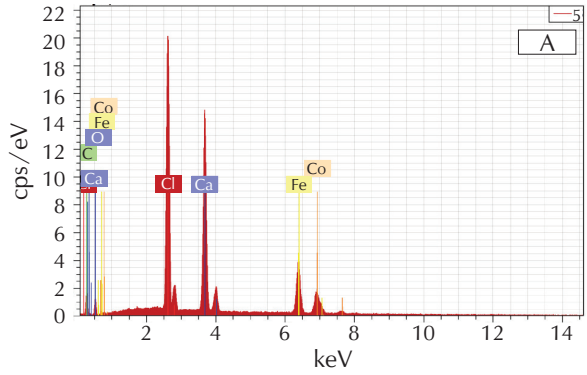

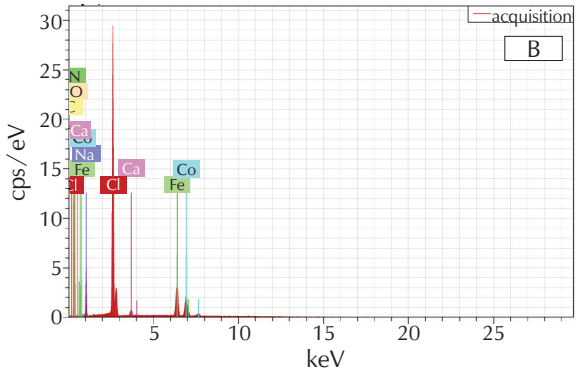

Element	Wt.%	Atom.%
Chlorine	17.98	11.28
Calcium	22.16	12.30
Carbon	26.14	48.42
Oxygen	14.81	20.60
Iron	11.98	4.77
Cobalt	6.94	2.62
Total	100.00	100.00

Element	Wt.%	Atom.%
Chlorine	41.99	30.92
Iron	9.79	4.58
Sodium	20.14	22.87
Cobalt	8.01	3.55
Calcium	1.52	0.99
Carbon	10.58	23.00
Oxygen	3.33	5.43
Nitrogen	4.65	**8.67**
Total	100.00	100.00

Fig. 6 – EDX micrographs of: A) alginate/$CoFe_2O_4$ beads, and B) macroporous urea grafted alginate/$CoFe_2O_4$ beads

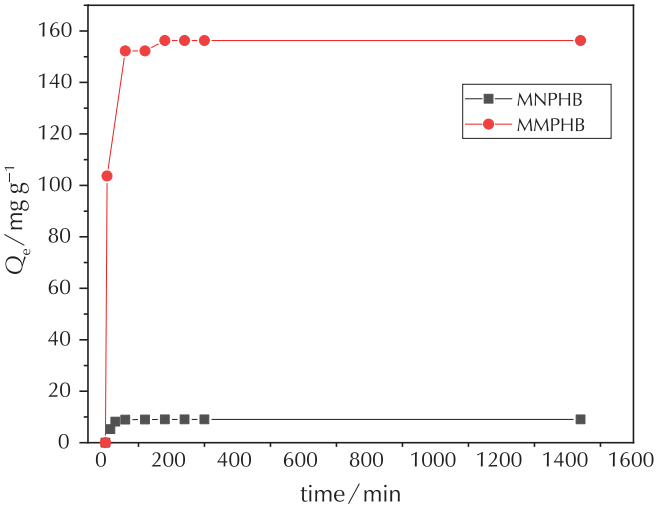

Fig. 7 – Adsorption capacity of salicylic acid on MNPHB and MMPHB as a time function

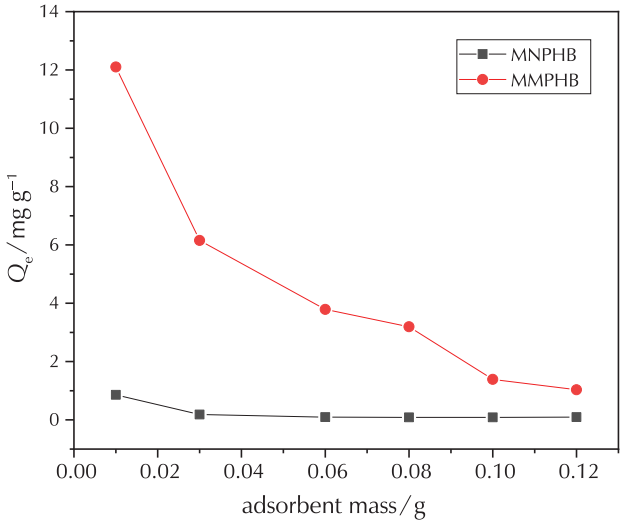

Fig. 8 – Adsorption capacity of salicylic acid on MNPHB and MMPHB as a function of the adsorbent mass

3.1.5 Energy Dispersive X-Ray Analysis

The elemental composition of alginate/$CoFe_2O_4$ and macroporous urea grafted alginate/$CoFe_2O_4$ beads is shown in the EDX micrographs in Fig. 6. The reaction between hydroxyl groups OH of alginate and the amine groups of urea produced the urea grafted alginate with release of ammonia. Analysing the results of EDX, the presence of nitrogen (8.67 atom%) was noticed in the composition of the urea grafted alginate/$CoFe_2O_4$ prepared beads, which confirmed the chemical modification of alginate with urea.

3.2 Study of salicylic acid adsorption on the prepared hybrid beads

The salicylic acid adsorption capacity on MNPHB and MMPHB as a time function is represented in Fig. 7. The obtained graph showed that the adsorption process had two distinct parts. The adsorption capacity increased rapidly during the first part (60 min) for the two forms of magnetic beads, until reaching values of 9.026 mg g^{-1} and 152.22 mg g^{-1} for MNPHB and MMPHB, respectively. Fig. 8 shows the adsorption capacity evolution as a function of the respective mass values of the MNPHB and

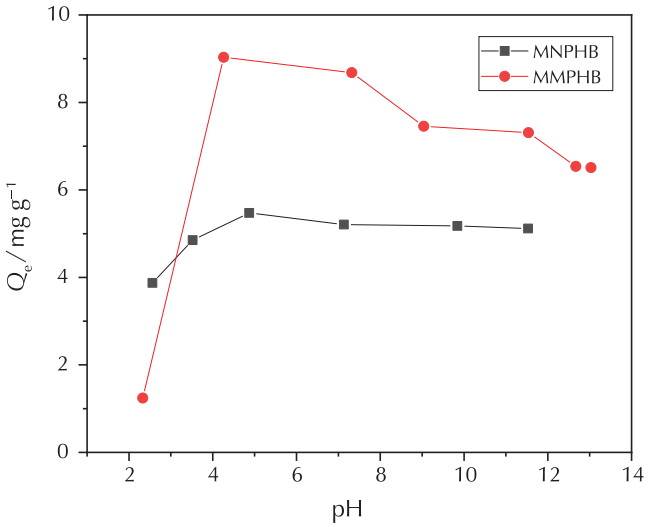

Fig. 9 – Adsorption capacity of salicylic acid on MNPHB and MMPHB as a function of pH

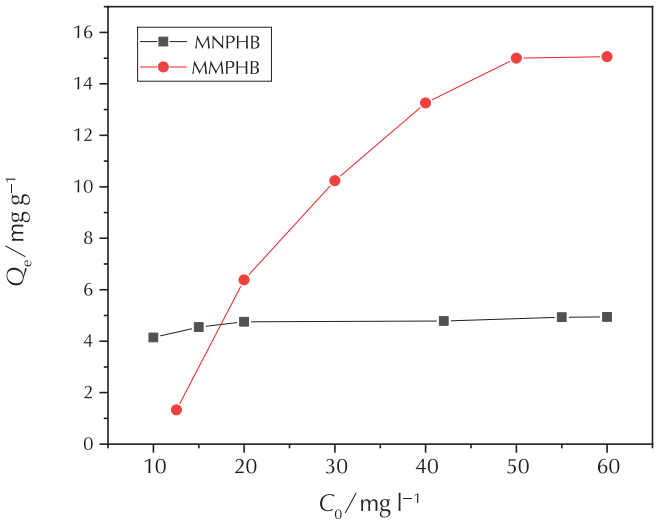

Fig. 10 – Adsorption capacity of salicylic acid on MNPHB and MMPHB as a function of C_0

MMPHB adsorbents. In this study, several adsorbent quantities were varied from 0.01 to 0.12 mg. It was observed that the adsorption capacity was maximal at 0.01 mg for the two adsorbents. This adsorption capacity decreased as the mass increased. This phenomenon may be explained by the unsaturation of the adsorption sites.

The influence of pH on the adsorption of salicylic acid is shown in Fig. 9. Analysing the figure, there is a rise in salicylic acid adsorption capacity until pH = 4 with an adsorption capacity of 5.47 mg g^{-1} and 9.03 mg g^{-1} for MNPHB and MMPHB, respectively. Beyond this pH value, a decrease in the adsorption capacity was noticed. This result can be explained by the fact that, for this pH value, which was lower than the isoelectric point of the adsorbents (pH_{pzc} = 7.02 and pH_{pzc} = 8.5), the beads surface was positively charged and the salicylic acid dissociated in salicylate anions (pK_a = 2.97). The rise in salicylic acid retention was probably due to the attractive interaction forces between the positively charged adsorbent and the negatively charged dissociated adsorbate. The decrease in the adsorption capacity at higher pH values may have been due to the repulsive interaction forces between the negatively charged adsorbent and the salicylate anions. The same results are endorsed by *Imessaoudene et al.*[24] and *Liadó et al.*[25]

The salicylic acid concentration was varied from 10 to 100 mg l^{-1}. Fig. 10 shows the evolution of the adsorption capacity of MNPHB and MMPHB according to C_0, the figure indicates that the adsorption capacity of MMPHB rapidly increased until an initial concentration value of 50 mg l^{-1} with an adsorption capacity of 15 mg g^{-1}.

3.3 Adsorption kinetics

Adsorption kinetics process is essential for wastewater treatment; it provides the necessary information on the solute retention percentage and the reaction pathways. The contact time effect on salicylic acid removal rate was monitored in this study.

Table 1 – Parameters of pseudo-first and pseudo-second order models for MNPHB and MMPHB

Reaction order	Parameters	Values of MNPHB	Values of MMPHB
	$q_{e(exp)}$ / mg g^{-1}	**9.02**	**152.22**
Pseudo-first order	$q_{e(cal)}$ / mg g^{-1}	1.96	13.54
	K_1 / min^{-1}	−0.00021	−0.00064
	R^2	**0.51**	**0.40**
	SSE	**0.30801**	**3.25825**
Pseudo-second order	$q_{e(cal)}$ / mg g^{-1}	9.27	152.25
	K_2 / g mg^{-1} min^{-1}	0.02444	0.60254
	R^2	**0.99965**	**0.99996**
	SSE	**0.02748**	**0.01720**

Analysing the results of Table 1, it was noted that the coefficients of determination (R^2) were higher and the SSE value lower for the pseudo-second order model than those for the pseudo-first order model. Therefore, q_e experimental values failed to match well with the calculated theoretical values for pseudo-first order model. Thus, the salicylic acid sorption mechanism onto MNPHB and MMPHB followed the pseudo-second order kinetics model, which implied that the adsorption phenomenon might have occurred *via* a chemical process involving valence forces that exchange or share electrons.

3.4 Adsorption isotherms

The results of plotting $q_e = f(c_e)$ are shown in Figs. 11 and 12. The extracted adsorption parameters from the non-linear plots of the Freundlich and Langmuir models after salicylic acid adsorption on the MMPHB are all summarized in Table 2. It was observed that Freundlich model

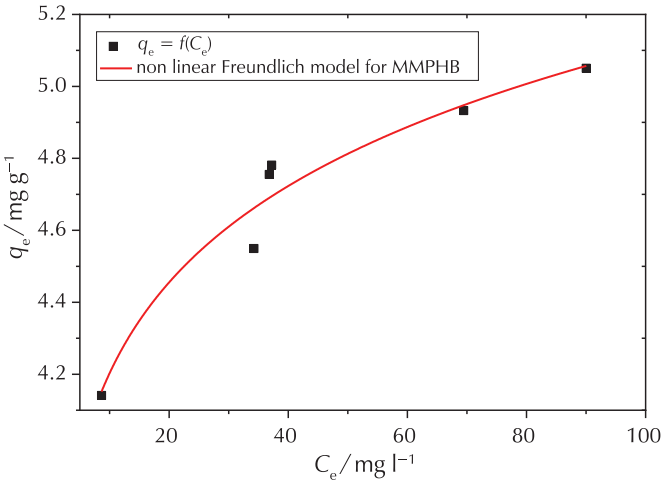

Fig. 11 – Modelling of salicylic acid adsorption onto MMPHB by Freundlich model

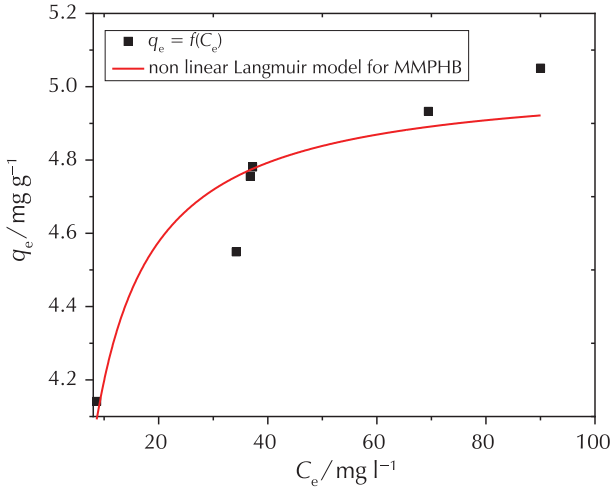

Fig. 12 – Modelling of salicylic acid adsorption onto MMPHB by Langmuir model.

Table 2 – Modelling parameters relating to Freundlich and Langmuir adsorption isotherms of salicylic acid

MMPHB	Freundlich model				Langmuir model			
	R^2	K_F	n	SSE	R^2	K_L	q_{max} / mg g^{-1}	SSE
	0.95	3.46	11.88	0.02478	0.84	0.50	5.02	0.06337

best described the predicted data. With the highest coefficient of determination (R^2 = 0.95) and the lowest SSE value (0.02478). These results showed that the adsorption of salicylic acid onto MMPHB fitted the Freundlich model better than the Langmuir model, which defines the surface heterogeneity and the exponential distribution of active sites and their energies.[19]

4 Conclusions

Magnetic nonporous hybrid beads MNPHB and magnetic macroporous hybrid beads MMPHB that were prepared using urea grafted alginate and cobalt ferrite, were used to remove salicylic acid emerging pollutants from contaminated water. The adsorption tests study has demonstrated the efficiency of the MNPHB and MMPHB biocomposites in salicylic acid removal, with adsorption capacities of 9.026 mg g^{-1} and 152.22 mg g^{-1} for MNPHB and MMPHB, respectively, for an equilibrium time period of 60 min, pH 4, adsorbent mass 10 mg, initial concentration of 10 mg l^{-1}, and temperature of 25 °C. The higher R^2 and the lower SSE values indicated that the adsorbate onto MNPHB and MMPHB followed a pseudo-second order kinetics model. The Freundlich isotherm was more suitable for the adsorption data. MMPHB biocomposites can be considered as a new material for removal of emerging pollutants from wastewater with high efficiency.

List of abbreviations

MNPHB – magnetic nonporous hybrid beads
MMPHB – magnetic macroporous hybrid beads
EPs – emerging pollutants
pH_{pzc} – point of zero charge
SSE – sum of squares of the errors

References
Literatura

1. *A. Carmalin Sophia, E. C. Lima*, Removal of emerging contaminants from the environment by adsorption, Ecotoxico. Environ. Saf. **150** (2018) 1–17, doi: https://doi.org/10.1016/j.ecoenv.2017.12.026.
2. *A. Gogoi, P. Mazumder, V. Kumar Tyagi, G. G. Tushara Chaminda, A. Kyoungjin An, M. Kumar*, Occurrence and Fate of Emerging Contaminants in Water Environment : A Review, Groundw. Sustain. Dev. **6** (2018) 169–180, doi: https://doi.org/10.1016/j.gsd.2017.12.009.
3. *J. Akhtar, N. A. S. Amin, K. Shahzad*, A review on removal of pharmaceuticals from water by adsorption, Desalination Water Treat. **57** (2015) 12842-12860, doi: https://doi.org/10.1080/19443994.2015.1051121.
4. *M. D. Vedenyapina, A. Y. Kurmysheva, A. K Rakishev, Y. G. Kryazhev*, Activated Carbon as Sorbents for Treatment of Pharmaceutical Wastewater (Review), Solid Fuel Chem. **53** (2019) 382–394, doi: https://doi.org/10.3103/S0361521919070061.
5. *I. Aroun, N. Bensacia, K. Seffah, S. Benyahia*, Kinetic and Equilibrium Studies of Salicylic acid Adsorption from Contaminated Water by (Alginate/Chitosan/Cobalt ferrite) Nanocomposites, Algerian J. Env. Sci. Technol. **5** (3) (2019) 1055–1061, www.aljest.webs.com.
6. *N. Bensacia, S.Moulay,* Functionalization of polyacrylic acid with tetrahydroxybenzene via a homolytic pathway: Application to metallic adsorption, Int. J. Polym. Mater. Polym. Biomater. **61** (9) (2012) 699–722, doi: https://doi.org/10.1080/00914037.2011.617343.
7. *K. Seffah, N. Bensacia, A. E. Skender, E. Flahaut, A. Hadj-ziane-zafour*, Synthesis and characterization of nano-magnetic material based on (carbon nanotubes/nickel ferrite): Application for the removal of methyl orange dye from contaminated water, Algerian J. Env. Sci. Technol. **3** (1) (2017) 45–53, doi: https://doi.org/10.1016/j.carbon.2013.06.006.
8. *V. C. Souza, M. G. N. Quadri*, Organic-inorganic hybrid membranes in separation processes: A 10-year review, Braz. J. Chem. Eng. **30** (4) (2013) 683–700, doi: https://doi.org/10.1590/S0104-66322013000400001.
9. *D. H. K Reddy,Y. Yun.* Spinel ferrite magnetic adsorbents: Alternative future materials for water purification?, Coord Chem Rev. **315** (2016) 90–111, doi: https://doi.org/10.1016/j.ccr.2016.01.012.
10. *L. Zhao, J. Basly, M. Baudu,* Macroporous alginate/ferrihydrite hybrid beads used to remove anionic dye in batch and fixed-bed reactors, J. Taiwan Inst. Chem. Eng. **74** (2017) 129–135, doi: https://doi.org/10.1016/j.jtice.2017.02.006.
11. *W. Jiao,W. Chen, Y. Mei, Y. Yun, B. Wang, Q. Zhong, H. Chen,* Effects of Molecular Weight and Guluronic Acid/Mannuronic Acid Ratio on the Rheological Behavior and Stabilizing Property of Sodium Alginate, Molecules **23** (2019) 4374–4386, doi: https://doi.org/10.3390/molecules24234374.
12. *F. Dehghani, S. Hashemian, A. Shibani,* Effect of calcination temperature for capability of MFe_2O_4 (M = Co, Ni and Zn) ferrite spinel for adsorption of bromophenol red, J. Ind. Eng. Chem. **48** (2017) 36–42, doi: https://doi.org/10.1016/j.jiec.2016.11.022.
13. *A. Benettayeb, E. Guibal, A. Morsli, R. Kessas,* Chemical modification of alginate for enhanced sorption of Cd(II), Cu(II) and Pb(II), Chem. Eng. J. **316** (2017) 704–714, doi: https://doi.org/10.1016/j.cej.2017.01.131.
14. *L. Sun, B. Fugetsu,* Graphene oxide captured for green use: Influence on the structures of calcium alginate and macroporous alginic beads and their application to aqueous removal of acridine orange, Chem. Eng. J. **240** (2013) 565–573, doi: https://doi.org/10.1016/j.cej.2013.10.083.
15. *K. Zhang, Y. Xu, X. Hua, H. Hania, J. Wanga, J. Wanga, Y. Liub, Z. Liu*. An intensified degradation of phenanthrene with macroporous alginate – lignin beads immobilized Phanerochaete chrysosporium, Biochem. Eng. J. **41** (2008) 251–257, doi: https://doi.org/10.1016/j.bej.2008.05.003.
16. *M. Davranche, S. Lacour, F. Bordas, J. C. Bollinger,* An easy determination of the surface chemical properties of simple and natural solids, J. Chem. Educ. **80** (1) (2003) 76–78, doi: https://doi.org/10.1021/ed080p76.
17. *A. O. Dada, A. P. Olalekan, A. M. Olatunya,* Langmuir, Freundlich, Temkin and Dubinin–Radushkevich Isotherms Studies of Equilibrium Sorption of Zn^{2+} Unto Phosphoric Acid Modified Rice Husk, IOSR J. Appl. Chem. **3** (1) (2012) 38–45, doi: https://doi.org/10.9790/5736-0313845.
18. *J. Wang, X. Guo,* Adsorption isotherm models: Classification, physical meaning, application and solving method, Chemosphere. **258** (2020) 127–179, doi: https://doi.org/10.1016/j.chemosphere.2020.127279.
19. *N. Ayawei, A. N Ebelegi, D. Wankasi,* Modelling and Interpretation of Adsorption Isotherms, J. Chem. **2017** (2017) 3039817, doi: https://doi.org/10.1155/2017/3039817.
20. *M. Chaker Ncibi,* Applicability of some statistical tools to predict optimum adsorption isotherm after linear and non-linear regression analysis, J. Hazard Mater **153** (2008) 207–212 doi: https://doi.org/10.1016/j.jhazmat.2007.08.038.
21. *Z. Tong, Y. Chen, Y. Liu, L. Tong, J. Chu, K. Xiao, Z. Zhou, W. Dong, X. Chu,* Preparation, characterization and properties of alginate/poly(γ-glutamic acid) composite microparticles, Mar. Drugs. **15** (4) (2017) 91, doi: https://doi.org/10.3390/md15040091.
22. *A. Sigdel, J. Lim, J. Park, H. Kwak, S. Min, K. Kim, H. Lee, C. H. Nahm, P. Park,* Immobilization of hydrous iron oxides in porous alginate beads for arsenic removal from water, Environ. Sci. Water Res. Technol. **4** (8) (2018) 1114–1123, doi: https://doi.org/10.1039/c8ew00084k.
23. *S. B. Waje, M. Hashim, W. D. W. Yusoff, Z. Abbas,* X-ray diffraction studies on crystallite size evolution of $CoFe_2O_4$ nanoparticles prepared using mechanical alloying and sintering, Appl. Surf. Sci. **256** (10) (2010) 3122–3127, doi: https://doi.org/10.1016/j.apsusc.2009.11.084.
24. *D. Imessaoudene, N. Bensacia, F. Chenoufi*, Removal of cobalt(II) from aqueous solution by spent green tealeaves, J. Radioanal. Nucl. Chem. **324** (3) (2020) 1245–1253, doi: https://doi.org/10.1007/s10967-020-07183-9.
25. *J. Liadó, M. Solé-Sardans, C. Lao-Luque, E. Fuente, B. Ruiz,* Removal of pharmaceutical industry pollutants by coal-based activated carbons, Process Saf. Environ. Prot. **104** (2016) 294–303, doi: https://doi.org/10.1016/j.psep.2016.09.009.

SAŽETAK

Sinteza i karakterizacija novih magnetičnih zrna za adsorpciju salicilne kiseline iz vodene otopine

Imane Aroun,[a] *Nabila Bensacia*,[a,b*] *Nadjet Taoualit*,[b] *Lylia Djadi*,[b] and *Amina Iakhlef*[b]

Istraživanje je usmjereno na sintezu dvaju pripremljenih oblika adsorbenta: magnetskičkih neporoznih hibridnih zrna (MNPHB) i magnetičnih makroporoznih hibridnih zrna (MMPHB). Ispitivanja adsorpcije salicilne kiseline na MNPHB i MMPHB provedena su pri temperaturi od 25 °C, pH-vrijednosti 4, masi adsorbenta od 10 mg i početnoj koncentraciji salicilne kiseline od 10 mg l^{-1}. Utvrđeno je da je adsorpcijski kapacitet MNPHP i MMPHB 9 mg g^{-1} odnosno 152 mg g^{-1}. Kinetika adsorpcije opisana je modelom pseudo-drugog reda i Freundlichovom izotermom za zrna MMPHB.

Ključne riječi
Adsorpcija, salicilna kiselina, nova onečišćivala, alginat cijepljen ureom, kobaltov ferit, magnetična makroporozna zrna

[a] *Laboratoire de Génie Chimique, Université de Blida 1, Bp270 route Soumaa, Blida (9000), Alžir*

[b] *Laboratoire des applications énergétiques de l'hydrogène, Université de Blida 1, Bp270 route Soumaa, Blida (9000), Alžir*

Izvorni znanstveni rad
Prispjelo 4. kolovoza 2021.
Prihvaćeno 28. rujna 2021.